Design of an Apparatus for Wind Tunnel Tests of Electric UAV Propulsion Systems

Miguel Borges
miguel.borges@ist.utl.pt

Instituto Superior Técnico, Lisboa, Portugal

June 2015

Abstract

The demand for alternative energy sources has grown in recent years. The shift to electricity can already be seen in the automotive industry, and the aviation industry is slowly follow the same path. This thesis focuses on the design, construction and validation of a system to test electrical propulsive systems capable of being used in unmanned aerial aircraft. The system developed was a test rig capable of testing electric motors with propellers with a maximum diameter of 27 inches. The measuring system installed on the test rig flexible enough to be able to perform measurements of different ranges generated by different propulsive systems. The experimental apparatus was installed in the aero-acoustic wind tunnel IST that allows out tests in a dynamic and static environment. All the mechanical design take into account the measurement limits previously studied according to data provided the propeller manufacturers. Through this test bench it is possible to generate the data for the propulsion system in a simple and flexible way. For this, it was created an interface so that the user can have access to all the generated data by the propulsion system in real time, but at the same time can also store that data for further post processing.

Keywords: UAV, Electric Propulsion, Test Rig, Wind Tunnel. Propeller Performance, Data Acquisition

1. Introduction

Nowadays, with the increasing price of fossil fuels, the demand for the usage of electricity has been rising in the past years. In the aviation industry, the development of unmanned airplanes has grown a lot not only because of their efficiency but also because of their agility and capability of adapting to almost every environment. The simplicity and improvement of their components made the Unmanned Aerial Vehicle (UAV) one of the most important tools for the mass emergence of unmanned vehicles[6].

These paper aims to make good use of the current computer capabilities to study the main features of the propulsion system of an UAV. With a well designed propulsive system, fitted to each different case, it will be possible to have a more efficient flight. To achieve this, it will be necessary to design a Test Rig. This design will be based on the physical testing limits that are proposed for this test bench. The complete structure will be assembled inside the aero-acoustic wind tunnel (WT) at IST. To measure all the output data produced by the motor, the test rig will be equipped with several sensors that will allow the user monitor and record all the data during a test.

The material presented here is part of a collaborative research project involving three research units belonging to the research line of Aeronautics and Space of LAETA, namely CCTAE, AEROG and IDMEC.These is part of project is entitled *Long Endurance Electric UAV* (LEEUAV)[7] and its goals are to develop a low cost, small footprint, easy to build and maintain multirole electric UAV, capable of being deployed from short airfields and able to adapt to different civilian surveillance missions.

2. Background

A significant advantage of electric motors is their rather vibration-free and quiet operation. A disadvantage has been their high weight per unit power output. With the advent of rare earth magnets, electric motors are now considerably lighter than two decades ago. For that reason, they are a candidate for propulsion of certain classes of vehicles. An example is the solar-cell/electric-motor/propeller system used in UAVs. A major problem with electric motor propulsion still is the weight associated with the energy storage (i.e. battery) and/or energy generation system.

2.1. Propeller Parameters

The important characteristic parameters of a propeller are its advance ratio, J, thrust coefficient C_T, torque coefficient C_Q, power coefficient C_P and the propeller efficiency η. Similar to many other aerodynamic problems, the aerodynamics of the propeller also make it convenient to express the thrust T, the torque Q, and the power P in suitable non-dimensional forms. If D represents the diameter of the propeller making N revolutions per unit of time, take the reference length as D, reference area as D^2, reference velocity as ND and the reference pressure as $\rho(ND)^2$. The non-dimensional coefficients of thrust,torque and power can be respectively, defined[9] as.

$$C_F = \frac{F}{\rho N^2 D^4}, \qquad C_Q = \frac{Q}{\rho N^2 D^5}, \qquad C_P = \frac{P}{\rho N^3 D^5}, \tag{1}$$

The propeller efficiency is an important characteristic parameter of the propeller arising due to its rotation in the air. It answers the question, how efficiently is the engine power (power input) converted to thrust power (power output). It is defined as the ratio between power output to power input.

$$\eta_T = \frac{P}{P_e} = \frac{FV}{Q_e 2\pi N}, \tag{2}$$

2.2. Test Rig Requirements

Before the test rig can be designed, it is necessary to establish what its testing limits will be. Our test stand will measure several data during each test, so it becomes necessary first to establish what will be the output/input data. As shown in Figure 1, the brushless motor, the wind tunnel, the ESC (Electronic Speed Controller) and the propeller tested will be associated to several measured parameters. Each of these parameters will be briefly described during this chapter including its maximum possible value.

The three main requirements that conditioned the maximum values measured in the test rig were:

- Propeller Diameter: Minimum 9", Maximum 27" .
- Motor diameter: 15-65 millimetres
- Wind tunnel speed: Maximum 50 m/s

Defined the three main constrains of our test stand, is now possible to present the limits for the test rig for each parameter (see table 1). This is very important since it will define the choice of sensors to be installed in the test rig.

Because the test rig is going to be mounted inside the aero-acoustic wind tunnel at IST, which is an anechoic chamber, it will only be available a limited space for fixing the structure to the ground. This will only be possible thanks to the grids that allow the users to walk inside the chamber (see figure 2 b)).

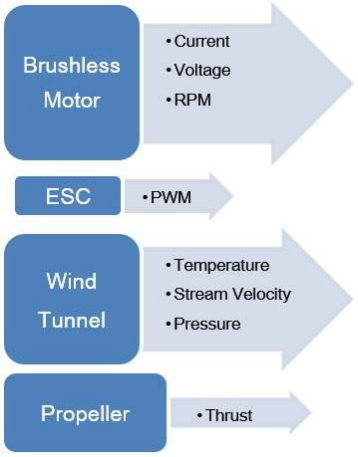

Figure 1: Output data taken from the system.

Measured Quantity	Min	Max
Interior Temperature	0°C	50°C
Motor Temperature	0°C	65°C
Thrust	0 Kg	30 Kg
Current	0 A	77.5 A
Tension	0 V	50 V
RPM	0 RPM	20000 RPM
Air Stream Velocity	0 m/s	30 m/s

Table 1: Summary of measured quantities and respective ranges

To achieve the requirement of the test rig be capable of testing propellers up to 27", it was necessary to limit the total height of the structure. To achieve always the best measurement possible, it was necessary that the centre of the propeller coincides always with the center of the wind tunnel nozzle. With this, it is possible to guarantee that the uniform flow coming from the wind tunnel nozzle is always covering the entire propeller. With this, it was possible to define the maximum height of the structure, around 1.3 meters.

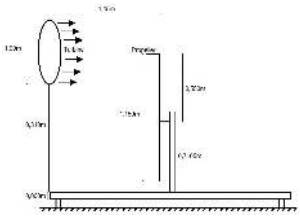

(a) Position of the test rig inside the tunnel

(b) Inside view

Figure 2: Test chamber of the aero-acoustic wind tunnel at IST

The support of the structure has to be centred according to the grid present inside the wind tunnel. As figure 3 a) shows, the structure have to be distanced around 1.45 meters from the wind tunnel nozzle.

The supports of the structure have also to conform the limits of the wind tunnel. As it is described in figure 3 and also represented before, the floor of the wind tunnel is not accessible due to the interior having been converted into an anechoic chamber. With this, it will only be possible to install the structure on the existing supports of the grids. According to figure 3 b), it assumed that the structure could only have a maximum of 0.68 meters in width.

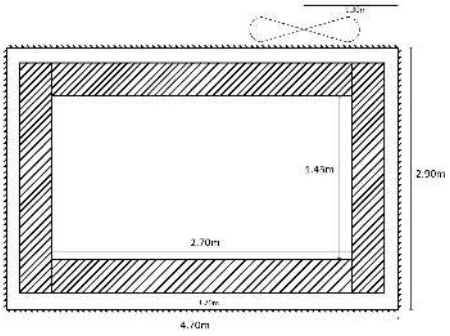

(a) Top view of test chamber

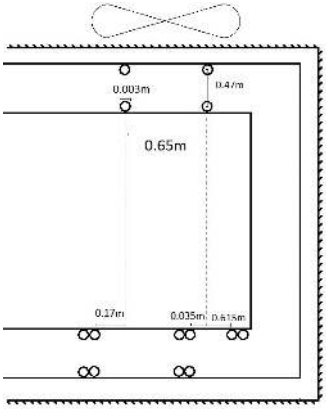

(b) Position of the test rig dimensions

Figure 3: Internal dimensions of the WT test chamber

3. Experimental Apparatus

3.1. Mechanical Design

After defining the main requirements of the test rig, is now possible to design and validate the proposed structure. The first assumption that was made was to install all the system in one main beam. This beam would have a pin, placed at mid height of the beam, that would have be the centre of rotation. This pin would be the part responsible for holding all the weight of the beam and its structure. Also this structure would have a variable load cell position so it can adjust the measure of the thrust to the tested propulsive system. Several ideas and version were created, however after after re-designinged these versions, it resulted in the structure represented in figure 4. The final structure was re-design in order to assembly correctly the load cell but also the bearing housing unit was rotated to a vertical position due to the advance of the main beam. With this, it was ensured a stable structure.

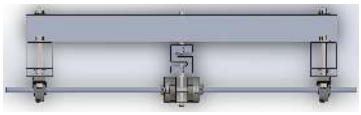

(a) Top view

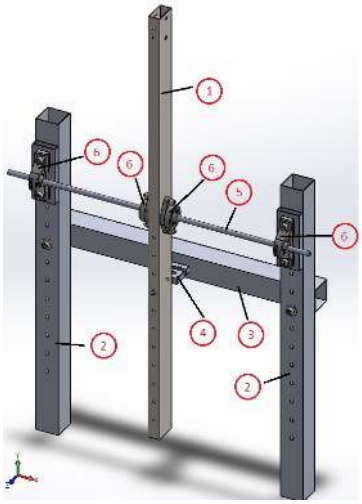

(b) Perspective view

Figure 4: Proposed solution for the measuring system of the test rig.

In figure 4 b), it is possible to see the several different components that the structure will contain. Table 2 briefly describes the components present in the structure.

Component	Name
1	Main beam
2	Support Beam
3	Rear beam
4	Load cell
5	Pin/Rod
6	Bearing Housing Unit

Table 2: Description of the components present in the structure

Also, as it was said previously, the load cell will have a variable position in the main beam. The value measured in the load cell will depend where the user of the test rig will position the load cell. In table 3 it is possible to see the available relations

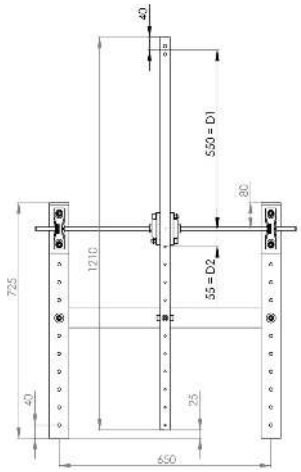

Figure 5: General dimensions for the structure.

for $\frac{D_1}{D_2}$ that this structure will have. Noting the the distance D_1 is the distance from the pin to the axis of the motor and the distance D_2 is the distance from the pin to the axis of the load cell.

Relation $\frac{D_1}{D_2}$
10
5
3.33
2.5
2
1.67
1.43
1.25
1.11
1
0.91

Table 3: Relations $\frac{D_1}{D_2}$ available in the main beam

It is also necessary to design the connection propeller-motor-beam. The main requirement for this connection was the flexibility that will allow to test different motors. With this, it was designed the structure presented in figure 6.

3.2. Support Foundation

Part of the experimental apparatus, was designed a simple foundation, represented on figure 7 a), having only three beams. These three beams will be attached one above the other.

3.3. Aerodynamic Shielding

Since the structure will be subjected to dynamic forces generated for the wind, it was necessary to design an aerodynamic structure, whose main purpose would be to protect the main beam from the wind to not influence the results measured. This shielding had to be enough aerodynamic to generate the lowest noise possible. Also, the vibration

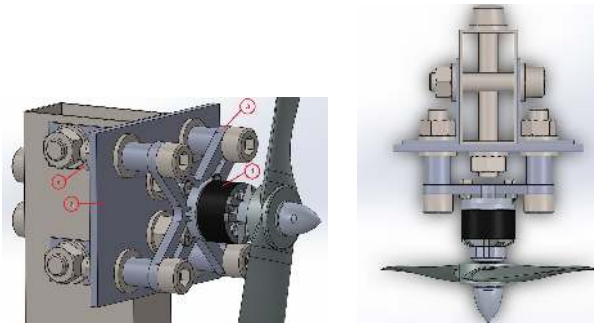

(a) Perspective view (b) Top view

Figure 6: Complete support structure for the motor in the main beam.

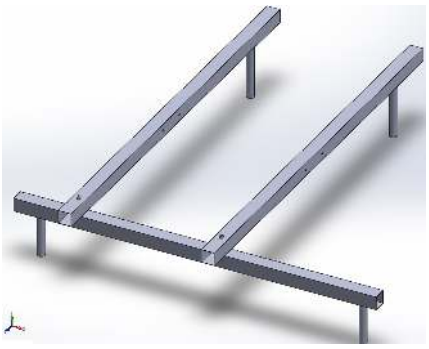

Figure 7: Test rig support foundation

generated by the wind passing through the shielding would generate vibrations that could add additional forces to the load cell or even damage the main beam. Thus, first it was decided to use a square aluminium beam 50x50 millimetres to accommodate the main beam. Choosing the material for this airfoil depended to the available cutting tools present in the laboratory. It was available a hot wire cutting machine in the laboratory equipped with CNC software. Thus, it was decided to use foam XPS, mainly used for coating of houses. This material present a good structural reliability but it is also easy to machine.

3.4. Final Design

After reviewed and build all the components, it was possible to assemble all the structural components in the wind tunnel. First it was mounted the structure without any sensors just to check if everything fitted correctly on the foundation. Then it was mounted the solid table that would allow to fix the wing and the user to stand near the test rig. Then finally the whole structure was mounted inside the wind tunnel. The final assembly is shown in figure 8.

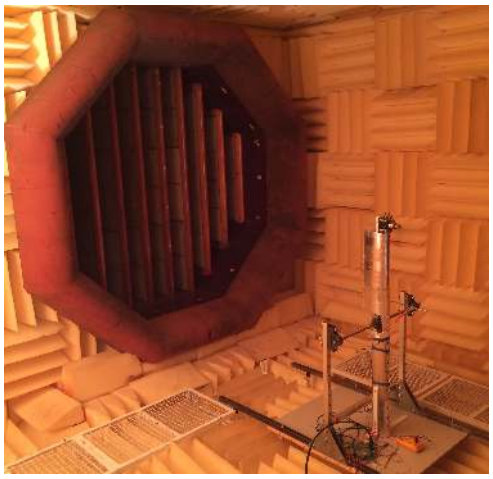

Figure 8: Final assembly of the test rig

3.5. Sensoring, Data Acquisition and Control

3.5.1 Load cell

For the load cell it was chosen a sensor that enables an assemble in the designed structure but also provides an adequate measuring range. It was chosen a S-type load cell from the manufacturer Vishay[3].The signal conditioner BA660[3] was used to amplify the analog voltage output of the load cell, from mv to V in order to have a better fillment of the range values.

(a) Load cell Vishay Model STC

(b) Signal Conditioner BA660

Figure 9: Load cell set.

3.5.2 Voltage and Current Sensor

After some research, it became apparent that the best solution was to use a sensor that could read both voltage and current, since it would simplify the wiring and lower the cost.In figure 10 it is possible to see the characteristics of the Pitlab 75A sensor[4] that was selected. It was chosen the 60 V version. Also in the same figure, it is represented the wiring layout for this sensor.

3.5.3 RPM Sensor

To measuring the RPM of the motor it was chosen the Reflective Optical Sensor with Transistor Output CNY70 from Vishay[3]. This sensor produced

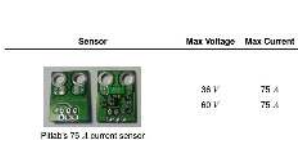

(a) 75A PitLab

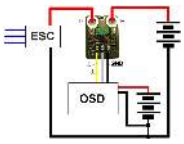

(b) Wiring layout

Figure 10: Voltage and current sensor.

stable RPM readings and the range of RPM allowed was also of large scale. The sensor was placed pointing to a reflective spot on the motor rotor. When rotating the sensor will generate a signal (and Voltage) with a different frequency. That change in frequency when multiplied by 60 (seconds in 1 minute) will give the exact number of RPM of the motor. In figure 11 it is possible to see the sensor used.

(a) Optical Sensor CNY 70 from Vishay

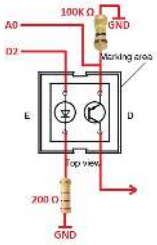

(b) Wiring layout

Figure 11: Reflective optical sensor Vishay CNY70.

3.5.4 Temperature

The temperature sensor was necessary for measuring the temperature of the air stream but also to measure the temperature of the motor. After market research, it was chosed the Thermocouple TMP36GZ produced by Analog Devices[2]. This Thermocouple allowed temperature from -40°C up to 125°C.

3.5.5 Air Speed Sensor

To measure the air stream speed a pitot tube was used. With the total and static pressure measured, the sensor gives the difference between both and then it is possible to compute the velocity through Bernoulli equation. The sensor used was a Freescale Semiconductor MPXV7002DP with two sensors integrated, one measures the static pressure and the other the total pressure. The sensor is shown in the Figure 12.

3.5.6 Motor Speed Control

For controlling the speed of the motor, as it was said before it is necessary to install an Electronic

Figure 12: Differential sensor Freescale Semiconductor MPXV7002DP

Speed Control(ESC). This device allows to control the speed of the motor through a PWM signal (Pulse Width Modulation). To ensure a better usage of the test rig, this control is performed through the LabView Interface. The input of the motor is a PWM signal with a frequency of 500 Hz, corresponding to a period of 2 ms. In the modulation, the duty cycle of the signal is varied so that 0% of duty cycle corresponds to 0% of throttle. This procedure is described in figure 13.

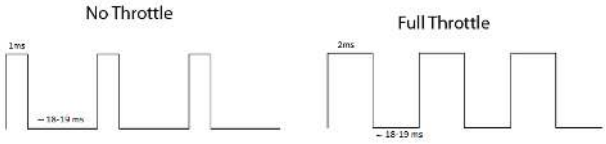

Figure 13: Signal evaluation according with the throttle delivered to the motor

3.5.7 Data Acquisition System

To read all the sensors outputs and record them, a data acquisition (DAQ) system will be used. This system will be comprised of a data acquisition board connected to a computer. The DAQ board, previously acquired, is the National Instrument NI PCIe-6321 (Figure 14)[5], which has 16 analogue +/-10 V inputs, connected to a computer running LabView, to read, convert and record the data acquired from the sensors.

(a) Hardware Board

(b) Pinout Squeme for the NI PCIe-6321

Figure 14: Nationals Instruments NI PCIe-6321[5]

3.5.8 User Interface

As it was discussed before, the user would have to be capable of working with the test rig in a simple way but also have to be capable of see the output data generated from the test rig. For this purpose, a graphical interface on the software LabView was created. This interface is shown in figure 15.

In this interface, before starting the test, the user needs to give the correct position of the load sensor using a select box with all the values of possible relations $\frac{D_1}{D_2}$. This is necessary since the correct thrust value depends on the position of the load cell. After this, the user can start the program. To increase the throttle of the motor, the user has a slide button which goes from 0% up to 100%. Then the program is equipped with several gauges that allow the user to see the different values measured with the sensors. All these files are recorded in file.

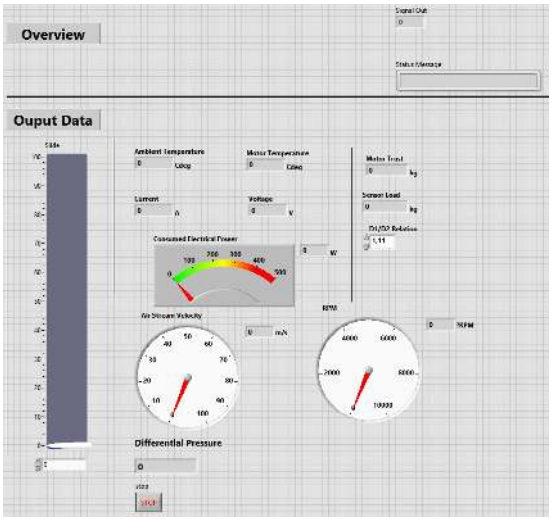

Figure 15: Graphical interface for operating the test rig

4. Results

After the assembly of all structural components of the test rig, and mounted and connected all sensors, it becomes necessary to test the test rig. All used sensors were calibrated whenever possible.

4.1. Sensor Calibration

4.1.1 Load Cell Sensor

To achieve a more correct measure for the load, due to the importance of this sensor, it was mounted a temporary structure near the test rig to calibrate it, ilustrated in figure 17. For this, known weights were used to generate the linear regression to apply for the load cell. It was mounted a sheave in front of the motor and attached a hire to it. The wire should be perfectly straight from the motor and the sheave in order to have a more accurate calibration. Then

the load cell was mounted in the position where the relation $\frac{D_1}{D_2}$ was unity. Without any weight, the load cell was zeroed by applying an offset in the LabView software where the measurement of all the sensors happens. Then five known weights were applied and then the values of the load cell were registered. The calibration plot is shown in figure 16.

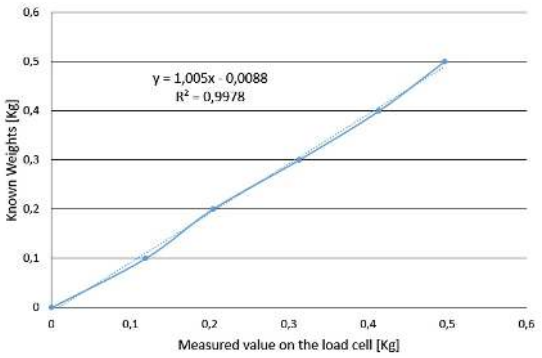

Figure 16: Load cell calibration and linear regression result.

Figure 17: Structure used for the calibration of the load cell

4.1.2 Current and Voltage Sensor

Both PitLab 36 V 75 A electrical sensors were calibrated using an available professional grade multimeter. To calibrate these sensors, two tests were executed. The first, aimed to calibrate the voltage sensor, was done by connecting both the sensor and the multimeter to a variable power supply, that could go from 12 V up to 30 V. Then the voltage was increased by 1 V, from 12 V to 30 V, and the readings from the multimeter and sensor were recorded.

After obtaining the data, it was plotted and a linear regression was used to obtain the calibration formula for the sensor. The results can be seen in figure 18. The current calibration was done using 12 V 21 W automotive light bulbs. The data acquisition program was the same as the previous test, as the program was made with both tests in mind. The data treatment was also done similarly to the voltage calibration.

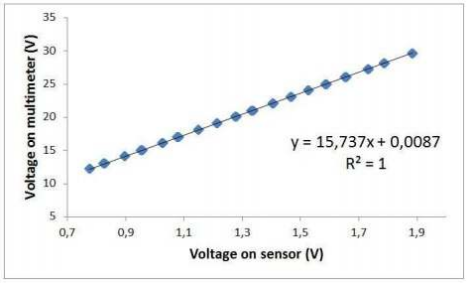

(a) Voltage calibration

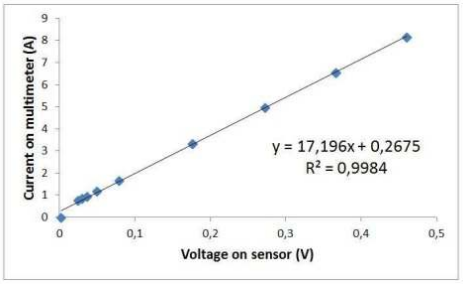

(b) Current calibration

Figure 18: Voltage and current sensors calibration.

The information from the manufacturer stated that these sensors had a voltage divider of 16:1 and a voltage to current conversion of 15.39 A measured (AM) per V output (VO). As can be seen in the previous results, figure 18 a), for this sensor the conversion factor for the voltage was 15.737 measured V per output V (VM/VO) with a zero offset of 0.0087 V, with a approximation factor of 100%. This result is very close to the manufacturer information. For the current sensor, the factory information was less accurate. As it can be seen in figure 18 b), the conversion factor is 17.196 AM/VO, quite far from the 15.39 AM/VO of the manufacturer, and an offset of 0.2675 A, which means that low current measure is not accurate enough to be considered valid. The approximation factor of the current linear regression is 99.84%, which is quite good. Both approximation factors are good, which means that the behaviour of the sensor is approximately linear.

4.1.3 Air Speed Sensor

The Pitot tube installed in the test rig was calibrated using a Pitot tube that was already installed in the wind tunnel and correctly calibrated. It was provided the relation between the frequency of the electrical motor that drives the wind tunnel fan and the true airspeed inside the tunnel. This information is shown in figure 19.

After this, the procedure done for calibrating this sensor was similar to the one performed for the load cell. First the sensor was reset so it can measure zero, and then a linear regression was applied based on the values presented in figure 19. Six measurements were done through the tests and the speed measured by the sensor was compared to the true value. The linear regression obtained is shown in figure 20.

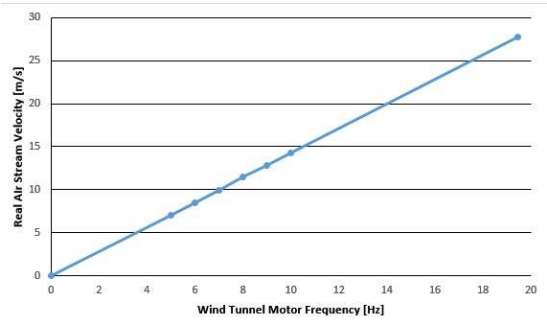

Figure 19: Relation of wind tunnel motor frequency with the true wind airspeed

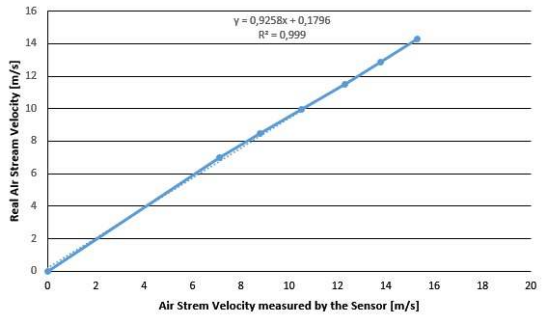

Figure 20: Linear regression applied to the airspeed sensor

4.2. Static Testing

For testing the test rig, due to the lack of time for testing more than one motor and propeller, it was decided to test the motor AXI 2826/10[8] assembled with an APC 14x7E[1] propeller. The static test was performed using only one run. The test rig was turned on and the throttle set at 10%. Then it was increased with 5% steps until reaching 85%. The results are shown above in figures 21 and 22.

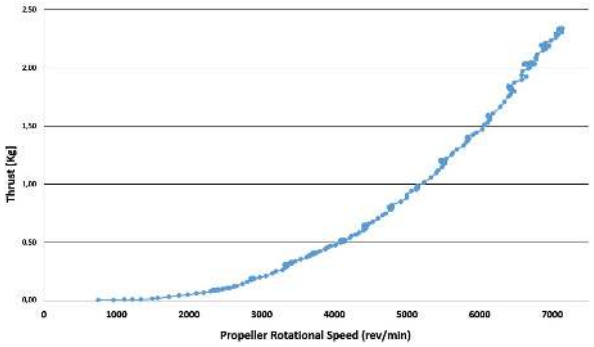

Figure 21: Thrust versus rev/min for the APC 14x7E propeller

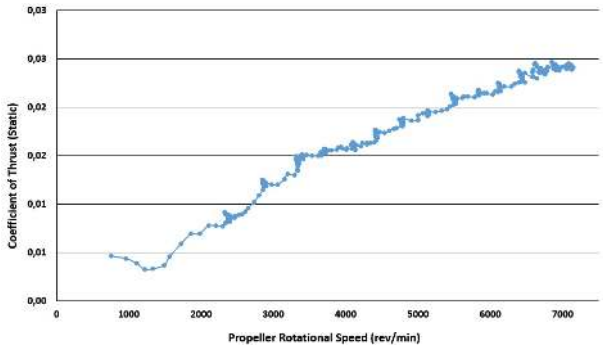

Figure 22: Thrust coefficient versus rev/min for the APC 14x7E propeller

For this type of motor during this test run it was consumed a maximum electrical power of 472W. This value was computed through the maximum current and voltage consumed during the test run. For the thrust generated, the maximum value registered was 0.028, producing a maximum thrust load of 2.465 Kg.f at 7100 RPM. To check the operability of the test rig, it becomes necessary to establish some reference to compare the results generated. For the propeller manufacturer APC[1], consulting their performance data for the selected propeller, at 7000 RPM the nominal thrust produced is 2.54 Kg.f producing a coefficient of thrust of 0.036. Thus, with this results, it is clear that it is possible to validate the test run performed as well the operability of the test rig.

4.3. Dynamic Testing

For the dynamic test, three tests were performed at different RPM. Each test consists in starting the motor and maintain it at a certain RPM and increasing the air stream velocity until the thrust generated by the system is null. This test was performed for a rotation of 3000, 5000 and 7000 RPM. The results are described in figures 23, 24 and 25. Similar to the static tests, the values generated were compared with the values given by

the propeller manufacturer APC[1]. For N=3000 rev/min, the propeller generated a coefficient of thrust, power and efficiency of 0.061, 0.033 and 0.0625 respectively. For N=5000 rev/min, the propeller generated a coefficient of thrust, power and efficiency of 0.0805, 0.0385 and 0.045 respectively. For N=7000 rev/min, the propeller generated a coefficient of thrust, power and efficiency of 0.08, 0.041 and 0.0425 respectively. As it is possible to see in all three figure, the plots were not constant during all the test runs. This was caused by some electromagnetic interferances that lead to perturbations in the recorded data. These perturbations could be caused by the wind tunnel, or even to the power supply of the motor.

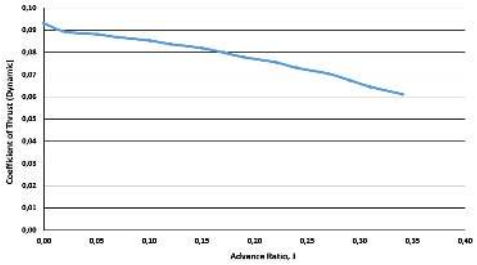

(a) Coefficient of Thrust versus Advance Ratio

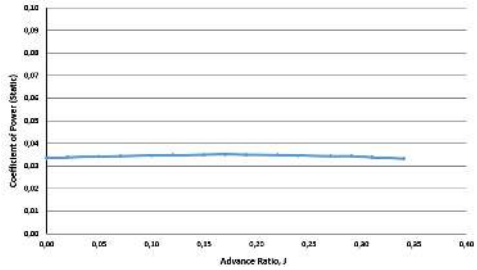

(b) Coefficient of Power versus Advance Ratio

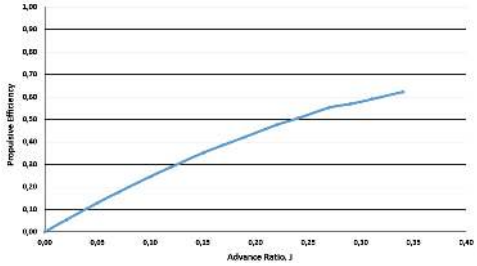

(c) Propulsive Efficiency versus Advance Ratio

Figure 23: Motor at N=3000 rev/min for the APC 14x7E propeller

5. Conclusions

The main goal of this thesis was the electro- mechanical project, construction and validation of a system that could allow the testing of an electric propulsion system to be used in UAVs. This system can be fitted in the LEEUAV Project. Of course, the propulsive system tested in the test rig

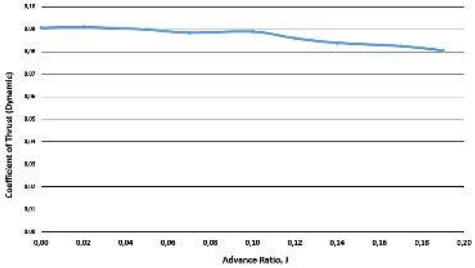

(a) Coefficient of Thrust versus Advance Ratio

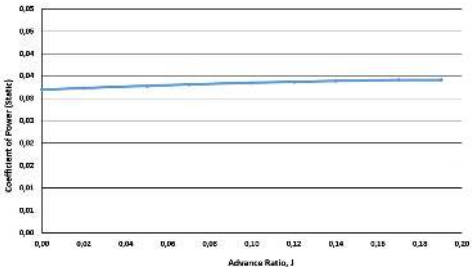

(b) Coefficient of Power versus Advance Ratio

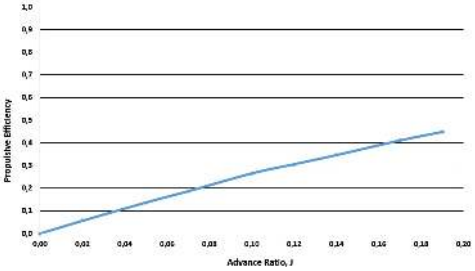

(c) Propulsive Efficiency versus Advance Ratio

Figure 24: Motor at N=5000 rev/min for the APC 14x7E propeller

can be applied to other UAV of bigger dimensions and higher electrical energy demand since the control is generic for any system and the type of test rig allows several different configurations of motor and propellers. The main conclusions achieved for this project were:

- The research made revealed that similar projects have lack of flexibility in terms of range of propellers and motors;
- Design, development and construction of a flexible structure that allows the test of several different ranges of propellers and brushless motors;
- Implementation of a graphical user interface based on the software LabView that allows the user of this test rig to have the reading and record of the output produced by the propulsive system;
- During the dynamic tests, the load produced by the wind generates a load that can seri-

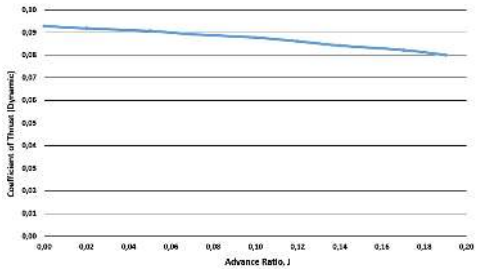

(a) Coefficient of Thrust versus Advance Ratio

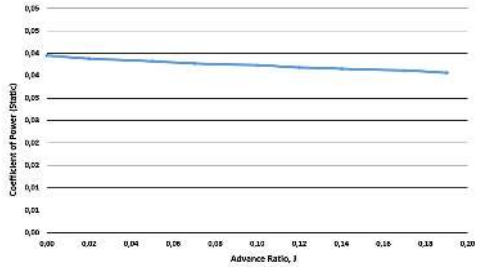

(b) Coefficient of Power versus Advance Ratio

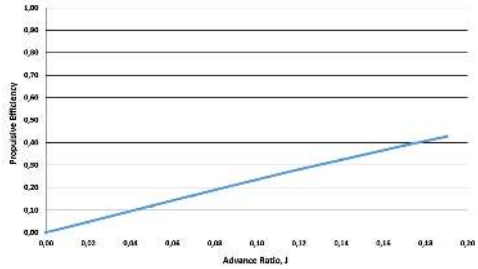

(c) Propulsive Efficiency versus Advance Ratio

Figure 25: Motor at N=7000 rev/min for the APC 14x7E propeller

ously compromise the thrust produced. However, the higher the air stream velocity passing through the blade of the propeller, the higher the propulsive efficiency

- Also, during the dynamic tests it was possible to see that the lower the rotation is, higher is the propulsive efficiency. Mainly because of the less drag produced by the airflow passing through the propeller;

5.1. Future Work

This project still has several features that can be improved. A better graphical user interface system can be introduced where the user after performing the static and dynamic tests can see the output plots corresponding to the propulsive system. Also a better data analysis can be introduced since the output data generated by the program contains a large size of information per each variable measured.

Also, since the amount of torque generated by this type of propulsive engine is high, a torque measuring system can be also introduced in the test rig.

Referring to the sensors used, it can be installed a more precise and stable sensor for measuring the air speed since it was the measure that gave more unprecise and unstable values comparing to the real values. Alternatively, different data filtering techniques can also be applied.

References

[1] A. A. P. Composites. *http://www.apcprop.com/*. Woodland, CA, USA.

[2] A. Devices. *http://www.analog.com/*. Massachusetts, USA.

[3] V. I. Inc. *http://www.vishay.com/*. Selb, Germany.

[4] P. innovative electronics. *http://www.pitlab.com/*. Warsaw, Poland.

[5] N. Instruments. *http://www.ni.com/*. Texas, USA.

[6] N. L. *Unmanned Aviation: A brief history of UAV's*. American Institute of Aeronautics and Astronautics, 2004.

[7] A. C. Marta and P. Gamboa. Long endurance electric uav for civilian surveillance missions. *29th Congress of the International Council of Aeronautic Sciences, St. Petersburg*, September 2014.

[8] A. M. Motors. *http://www.modelmotors.cz*. Pardubice, Czech Republic.

[9] S. K. Ojha. *Flight Performance of Aircraft*. Ed. Bombay, India: AIAA, 1st edition, 1995.